Research Square

Preprints are preliminary reports that have not undergone peer review.
They should not be considered conclusive, used to inform clinical practice,
or referenced by the media as validated information.

Glass-Nanofiber-Reinforced Strontium Aluminate/Epoxy Nanocomposite Coatings for Ceramics: Persistent Luminescence and Multifunctional Surface Protection

Ashraf H. Mourad
Cairo University
Meram S. Abdelrahman
National Research Centre
Tawfik A. Khattab
National Research Centre
Yasser A. Attia
yasserniles@niles.edu.eg

Cairo University

Research Article

Keywords: Electrospun glass fibers, Glazed polyepoxide, Nanocomposite coating, Photoluminescent ceramic, Antibacterial activity

Posted Date: November 20th, 2026

DOI: https://doi.org/10.21203/rs.3.rs-11658254/v1

License: This work is licensed under a Creative Commons Attribution 4.0 International License.
Read Full License

Additional Declarations: No competing interests reported.

Glass-Nanofiber-Reinforced Strontium Aluminate/Epoxy Nanocomposite Coatings for Ceramics: Persistent Luminescence and Multifunctional Surface Protection

Ashraf H. Mourad[a], Meram S. Abdelrahman[b], Tawfik A. Khattab[b], Yasser A. Attia[a,*]

[a] *National Institute of Laser Enhanced Sciences, Cairo University, Giza 12613, Egypt.*
[b] *Dyeing, Printing and Auxiliaries Department, Textile Research and Technology Institute, National Research Centre, Cairo 12622, Egypt.*

[**]Corresponding author: Yasser A. Attia (yasserniles@niles.edu.eg) Tel: +201129061463

ORCID ID: **http://orcid.org/0000-0002-5830-2250**

Emails: Ashraf.Mourad365@gmail.com; ms.abdel-rahman@nrc.sci.eg; ta.khattab@nrc.sci.eg; yasserniles@niles.edu.eg

Abstract

A multifunctional photoluminescent nanocomposite coating for ceramic substrates was developed using epoxy resin (EPR) as the polymeric matrix, strontium aluminate nanoparticles (NSA; 9–18 nm) as the photoluminescent component, and glass nanofibers (50–220 nm) as a reinforcing phase. The incorporation of glass nanofibers was designed to enhance the mechanical performance of the epoxy coating while maintaining its optical functionality. The morphological, structural, and surface characteristics of NSA, glass nanofibers, and NSA@EPR-coated ceramic films were systematically investigated using complementary analytical techniques. The resulting coatings exhibited high transparency under daylight, a green emission under UV irradiation, and a greenish-yellow afterglow in darkness. Upon excitation at 365 nm, the photoluminescent coatings displayed characteristic emission bands at 519 nm, corresponding to a strong green emission, and 438 nm, attributed to a weaker blue emission. Increasing the NSA loading progressively enhanced both the fluorescence intensity and long-persistent phosphorescence of the coatings. In addition to their photoluminescent behavior, the nanocomposite coatings demonstrated improved UV-shielding capability, scratch resistance, antibacterial activity, and hydrophobicity. The NSA-containing coatings also exhibited good durability and photostability, indicating their potential as robust multifunctional ceramic coatings for protective, decorative, and optical applications.

Keywords: Electrospun glass fibers; Glazed polyepoxide; Nanocomposite coating; Photoluminescent ceramic; Antibacterial activity.

1. Introduction

Photochromic compounds can reversibly alter their absorbance and/or emission properties upon exposure to light. Photochromic agents have been divided into two distinct groups, including materials capable of switching color in response to visible illumination and ultraviolet radiation [1-3]. Fluorescent coatings emit light upon exposure to an ultraviolet source and then return to their original state upon cessation of the irradiation source [4]. Phosphorescent coatings produce light for extended durations after the cessation of the lighting source [5]. Photoluminescence has garnered important attention owing to its potential uses in several fields, such as ophthalmic lenses, sensors, and optical data storage. Photochromism has displayed benefits in various applications, including military camouflage, trademark protection, electronic displays, security printing, and traffic signs [6-9].

Thin films have 2D layers with exceptional flexibility, lightweight, and extensive surface area, which provide enhanced elasticity and strength relative to conventional 3D dense materials [10, 11]. They are essential for numerous applications, providing a cost-effective preparation method that requires low raw ingredients while meeting crucial specifications. They have shown various characteristics for various applications, including medicinal agents, photovoltaics, UV filtration systems, antibacterial products, electronic devices, anticounterfeiting, hydrophobic surfaces, and antireflective coatings [12-15]. Nanoparticles have been utilized to provide enhanced features for polymeric substrates. Consequently, nanoparticle-containing nanocomposite films have garnered substantial interest owing to their beneficial characteristics, such as optical characteristics, sensory capabilities, water repellency, catalytic activity, transparency, electroconductivity, and antimicrobial efficacy, rendering them suitable for a variety of applications [16]. Luminescent films can be created by the integration of organic compounds, such as spiroxamine-derived dyes, in polymer substrates. Nevertheless, photoluminescent organic compounds provide some shortcomings, including limited photostability, photodegradation, and diminished photochromism due to steric effects [17, 18]. Inorganic phosphors, such as NSA, demonstrated ease of handling, durability, photostability, and enhanced mechanical properties [19]. Unlike organic molecules, inorganic agents remain impervious to photochromism, since their photophysical properties do not depend on molecular switches [20]. NSA has been used in numerous marketable goods due to its effective afterglow emission. It has been used in the creation of diverse technological items, including switching systems and traffic signals [21-23]. Various lanthanide-based phosphors have been developed as primary color-emitting agents, such as $Y_2O_2S:Mg^{2+}/Eu^{3+}/Ti^{4+}$ for red [24], $CaAl_2O_4:Eu^{2+}/Nd^{3+}$ for blue [25], and $SrAl_2O_4:Eu^{2+}/Dy^{3+}$ for green [26]. NSA exhibits nontoxicity, remarkable long-lasting phosphorescence (>10 h), recyclability, chemical resistance, efficient photoluminescence, non-radioactivity, superior photostability, and thermal stability [27].

Various smart coatings were studied for ceramics to improve their thermal, mechanical, and functional properties. Thus, luminescent ceramics necessitate the preparation of innovative coatings to allow considerable photostability for diverse residential and industrial applications [28]. Polymer coatings have gained considerable attention owing to their excellent mechanical qualities, including hardness [29]. Various commercial nanoparticles, such as carbon nanotubes and graphite, have been employed in various polymers to develop multifunctional coatings for numerous applications, such as cosmetics, agriculture, optics, catalysis, aerospace, medicine, and textiles [30-33]. Epoxy resins are active polymers noted for their beneficial physical features, such as elevated temperature stability, water resistance, non-

shrinking curing process, and superior mechanical strength. Consequently, it is used in several fields, including metal coatings, electrical insulation, adhesives, fiberglass wall panels, and electronics [34, 35]. Epoxy resins can function as coatings on various surfaces, providing exceptional transparency and significant aging resistance [36].

This work presents the first investigation into room temperature synthesis and use of smart coatings derived from a combination of epoxy and NSA toward efficient fabrication of resilient photoluminescent ceramics with mechanical reliability, abrasion resistance, and super hydrophobicity. The afterglow layer showed transparency in the white spectrum and green beneath UV light. NSA was analyzed by transmission electron microscopy (TEM) and X-ray diffraction (XRD). The ceramic morphology was examined by scanning electron microscopy (SEM), X-ray fluorescence (XRF), and energy-dispersive X-ray spectroscopy (EDX). The superhydrophobic features were assessed by recording the contact and sliding angles. The mechanical behavior of ceramics was examined. The ceramic coatings showed better scratch resistance and hydrophobicity upon increasing the NSA content in the glazed epoxy matrix. Coatings with larger NSA ratios persisted to emit green afterglow after the illumination supply was switched off, while coatings with lower NSA contents emitted green fluorescence when exposed to an irradiation supply. Consequently, there are a wide variety of ceramics that can profit from the use of the current coatings, such as building facades, electricity-free lighting, directional road signs, functional surfaces, and anti-counterfeiting labeling.

2. Experimental

2.1 Materials

Tetraethyl orthosilicate (TEOS; ≥99.0%), titanium dioxide nanoparticles (TiO_2; ≥99%), polyvinylpyrrolidone (PVP; Mw 1,300,000 by LS), dysprosium oxide (Dy_2O_3; 99.9%), dimethyl sulfoxide (DMSO; 99.9%), silicon dioxide (SiO_2; 99.8%), 3-glycidyloxypropyltrimethoxysilane (GPTMS; ≥98%), aluminum oxide (Al_2O_3; 99.99%), europium oxide (Eu_2O_3; 99.9%), 3-aminopropyl triethoxysilane (APTES; ≥98.0%), strontium carbonate ($SrCO_3$; ≥99%), dimethylformamide (DMF; 99.8%), and boric acid (H_3BO_3; ≥99.5%) were obtained from Sigma-Aldrich (Egypt). Epoxy resin (Kemapoxy 150-3D, 1.11±0.02 kg/L, colorless, and solvent-free fluid) and related hardener were acquired from Chemicals for Modern Building Company (Egypt). Ceramics, measuring 1.5 cm in width, 1.5 cm in length, and 1.0 cm in thickness, were procured from the local market (Egypt). The electrospinning of glass fibers was performed by using a formerly published procedure [19]. NSA was obtained by the top-down and solid-state reaction procedures [23].

2.2. Electrospinning of glass fibers

A combination of TEOS (3.75 g) and PVP (3.75 g) in a solvent mixture of DMF/DMSO (2:1; 25 mL) was stirred for 15 minutes and ultrasonicated at 25 kHz for 30 minutes. The given mixture was exposed to pyrolysis at 850 °C. A syringe needle (0.8 mm) connected to a plastic syringe positioned on a pump (WZ-500C2, Zhejiang, China) was utilized to discharge nanofibers into a collector at a flow rate of 6 mL/h and a voltage of 30 kV. The needle tip and the collector were set to 18 cm. **Figure 1** displays a schematic illustration for the electrospinning tool. Then, the provided fibers underwent a salinization process by treating the silanol substituent with silane toward an improved nanofiber affinity for the polyepoxide resin. The fibers (10 g) were stirred in distilled water (200 mL) and then ultrasonicated for 15 minutes. After filtration under vacuum, an ethanol solution of the fibers in silane (15%) was stirred at 45 °C for an hour. After filtration under vacuum, the fibers were stored in a desiccator for analysis.

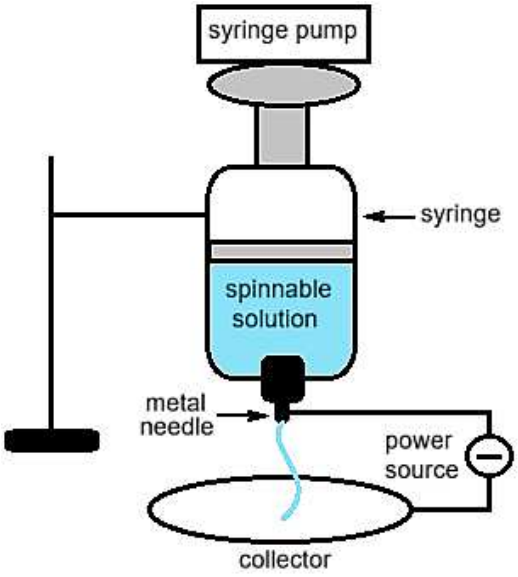


Figure 1. Scheme represents the electrospinning apparatus.

2.3. Synthesis of pigment nanoparticles

A mixture of H_3BO_3 (0.02 mmol), Eu_2O_3 (0.002 mmol), Dy_2O_3 (0.001 mmol), Al_2O_3 (0.2 mmol), and $SrCO_3$ (0.1 mmol) absolute ethanol (100 mL) was stirred for 2 hours. A homogeneous suspension was obtained by homogenizing the above solution at 25 kHz in 30 minutes. After a day of drying at 100 °C, the suspension went through 4 hours of grinding and 3 hours of sintering at 1250 °C. The supplied micro powder (1-15 μm) was added to a ball mill vial that was attached to a vibrating stage. Using the top-down method, the phosphor nanoparticles were produced by subjecting another ball mill to continuous smashes with the phosphor powder and the stage for 24 hours.

2.4. Ceramic coating

In a clean bowl, a mixture of TiO_2 (2.5% w/w; antimicrobial agent), glass fibers (5% w/w; glazing), epoxy (100 mL), and Al_2O_3 (2.5% w/w; reinforcement and stabilization) was combined with diverse quantities of NSA (w/w), including 0% (NSA_0), 0.25% (NSA_1), 0.5% (NSA_2), 1% (NSA_3), 2% (NSA_4), 4% (NSA_5), 6% (NSA_6), 8% (NSA_7), 10% (NSA_8), 12% (NSA_9), and 14% (NSA_{10}). Each solution was stirred for 2 hours and ultrasonicated (Vibra-Cell Ultrasonicator) at 30 kHz for an hour to achieve a consistent distribution of NSA free from lumps and air bubbles. The hardening substrate (30% w/w) gradually poured into every combination, stirred for 30 minutes, and sonicated at 20 kHz for 30 minutes. The sample was sonicated in a water bath for 30 minutes, treated with detergent, and dried for 40 minutes at 80 °C. The obtained nanocomposite was uniformly coated onto a ceramic surface by a roller and then dried for 11 hours at room temperature. In addition, the composites were subjected to casting on Teflon plates and dried for 11 hours at room temperature, providing transparent films with 1.5 cm in length, 1 mm in thickness, and 1.5 cm in width.

2.5. Analysis methods

A Bruker Advance D8 (Germany) was employed to conduct the XRD analysis of NSA. A JEM-2100 (Japan) was employed to analyze the size and shape of NSA. The TEM study was conducted by ultrasonicating an aqueous solution of NSA at 20 kHz for 60 minutes. The software on the TEM tool was used to determine the particle diameter. The elemental compositions of ceramics were measured by a VEGA3 TESCAN (Czech Republic) coupled to a TEAM

EDX analysis tool. In addition, a sequential Axios (Netherlands) was employed to explore the chemical analysis of coatings. A JASCO FP-8300 (Japan) connected with an exterior accessory was employed to explore the photophysical properties. To inspect the photostability and resistance to fatigue, the coated ceramics were subjected to 15 s and 150 s of irradiation under ultraviolet lamp (6 W). The sample was left in a dark chamber for an hour. The previous steps were repeated for several cycles, while the emission readout was measured. Using a Shimadzu spectrophotometer (UV-3600), the optical transmittance of films was determined. A HunterLab UltraScan Pro (USA) was utilized to study the CIE Lab system and color strength (*K/S*) of cast films. The CIE Lab coordinates are signified by b^* for the yellow (+)-to-blue (–) coordinate, a^* for the green (–)-to-red (+) coordinate, and L^* for the white (100)-to-black (0) coordinate [37]. A Shimadzu tool (ASTM:D638M) [38] and scratch pencils [39] were employed to measure the tensile strength and resistance to scratches, respectively. According to a standard process (AATCC:183:2010) [40], the capability of a film to block ultraviolet radiation was evaluated by measuring its Ultraviolet Protection Factor (UPF). A Dataphysics OCA15EC (Germany) was utilized to record the contact angle [41]. Both *E. coli* and *S. aureus* were used to examine the biological activity for the coated ceramics employing the biological counting approach (AATCC:100:1999). The antibacterial tests were performed under equivalent conditions, including illumination, temperature, and time [42, 43].

3. Results and discussion

3.1. Optical studies

Figure 2 displays a cast film (NSA_7) under different light conditions. Fluorescence was observed for ceramic surfaces with lower NSA contents (NSA_1–NSA_3) under ultraviolet light, which demonstrated rapid reversibility after switching off the ultraviolet source. The ceramic samples with higher NSA contents (NSA_4–NSA_{10}) exhibited slower reversibility after the illumination source was turned off, suggesting long-lasting photoluminescence. Because of its fluorescence and afterglow emissions, the produced glazed polyepoxide nanocomposite has several potential applications as a thin film in anticounterfeiting materials. The glazed polyepoxide nanocomposite (NSA_7) can be used to make gaskets with a specific pattern. This gasket emits a green light beneath UV rays, although this light is not detectable in the visible light. The optical transmittance for the glazed polyepoxide cast films was examined. It was observed to drop from 79% to 68% when the NSA concentration was raised from NSA_1 to NSA_{10}. For this reason, the present glazed polyepoxide can be presented as a potential candidate for anticounterfeiting labeling. **Figure 3a-b** shows the findings of analyzing the excitation and emission profiles. As the phosphor concentration was raised, the excitation band (365 nm) became stronger. With an increase in the UV exposure from 15 s to 150 s, the emission intensity (519 nm) was found to increase. Two emission intensities were noted in the visible spectrum, including 438 nm (weak peak of bluish emission) and 519 nm (strong peak of greenish emission). Nevertheless, the blue band (438 nm) diminishes at room temperature by thermal quenching [44]. A colorimetric shift from transparent to green was monitored in the presence of UV irradiation and to greenish yellow in a darkened room. The luminescent ceramics exhibited wide excitation and emission bands, including 250-500 nm and 350-675 nm, respectively. The emission intensity was monitored at 519 nm, which is the same as the phosphor nanopowder [26], as illustrated in **Figure 3c**.

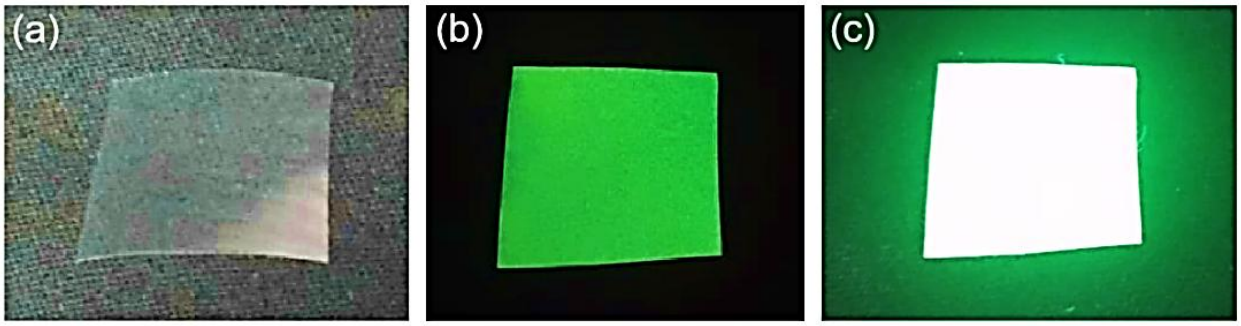


Figure 2. Photographic images of a cast film (NSA_7), showing a colorless appearance in the visible spectrum (a), greenish yellow phosphorescence in a dark place (b), and green emission under UV rays (c).

The transition of Eu^{2+} [$4f^6 5d^1 \leftrightarrow 4f^7$] is accountable for the NSA emission [20]. The absence of an identifiable phosphorescence peak for Eu^{3+} proposes that it has transformed into Eu^{2+} [20, 27]. Additionally, this proved that the light absorbed by Dy^{3+} transfers to Eu^{2+}. Dy^{3+} creates traps able to transmit energy to Eu^{2+}, generating emission as Eu^{2+} reverts to its ground position [27]. Effective luminous compounds usually show a strong resilience to depletion. After numerous cycles of ultraviolet illumination, the emission band of NSA_7 was monitored at 519 nm. After exposure to ultraviolet rays, NSA_7 was left in a dark place to emit a greenish yellow light for an hour, allowing NSA_7 to slowly return to its transparent state. By quantifying the emission band at 519 nm after every cycle, the coating showed high photostability and great reversibility **(Figure 3d)**. A nonlinear relationship was observed between the decay profiles, demonstrating two distinctive stages, as illustrated in **Figure 4**. Due to the brief period required to maintain electrons in the excitation state of Eu^{2+}, the first stage was rapid. The next stage was slow owing to the limited and shallow energy levels of Dy^{3+}. The emission period of rare-earth elements can be significantly prolonged due to their efficiency as entrapments [6].

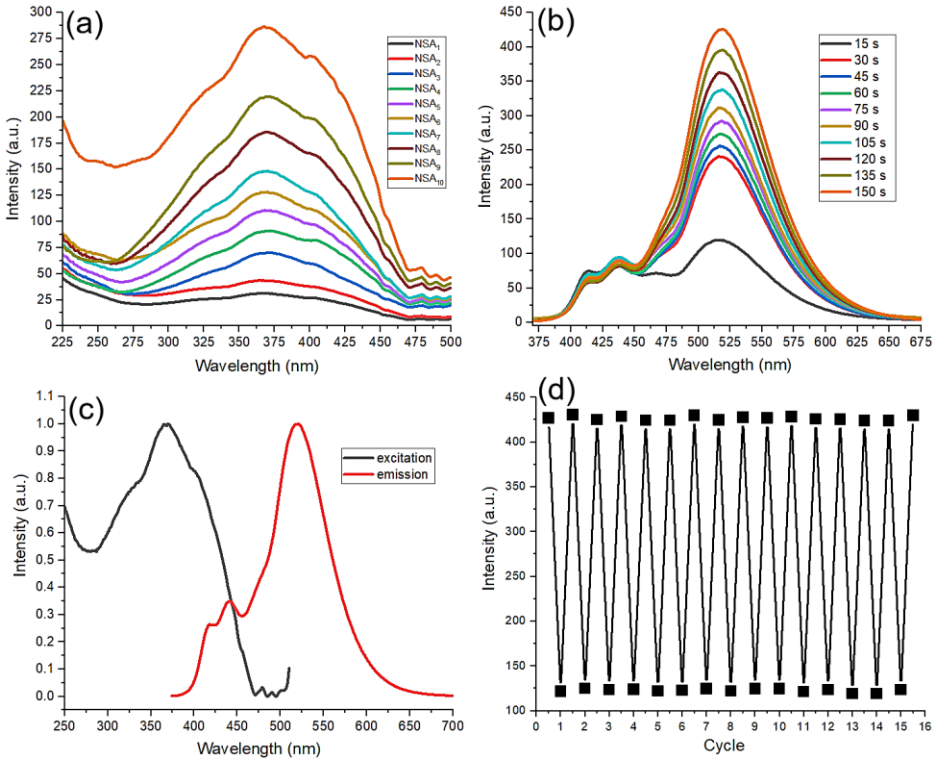


Figure 3. Excitation analysis of ceramics (a), emission analysis of NSA_7 against the ultraviolet excitation period (b), emission intensity of ceramic (NSA_7) at 519 nm after several cycles of ultraviolet excitation (c), and decay time of ceramics (d).

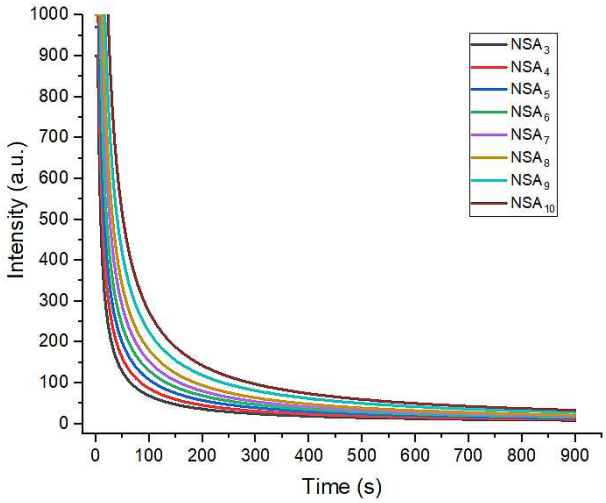


Figure 4. Decay time profiles of coated ceramics.

3.2. Appearance evaluation

Table 1 shows the results of the color evaluation conducted on cast films. To prepare a transparent coating, it is essential to ensure that NSA is evenly distributed throughout the polyepoxide coating. A green fluorescence was produced by the cast films containing lower concentrations of NSA, ranging from NSA_1 to NSA_3. On the other hand, cast films containing NSA at concentrations ranging from NSA_4 to NSA_{10} demonstrated long-persistent

photoluminescence. Due to their ability to preserve matrix transparency, nanoscale materials have lately garnered significant interest as fillers. Slight differences in *K/S* were observed when the NSA content increased from NSA_0 to NSA_{10}, confirming the coating transparency. When the NSA ratio was raised, the CIE Lab values, including L^*, a^*, and b^*, showed minor differences in the cast films, confirming their transparency.

Table 1. Appearance screening of cast films.

Parameter	NSA_0	NSA_1	NSA_2	NSA_3	NSA_4	NSA_5	NSA_6	NSA_7	NSA_7	NSA_9	NSA_{10}
a^*	–3.91	–3.76	–3.59	–3.34	–3.22	–3.06	–2.85	–2.49	–2.04	–1.66	–1.37
b^*	21.25	20.44	19.47	18.95	16.51	15.47	13.81	12.04	11.64	9.92	9.33
L^*	92.06	91.68	91.27	90.83	90.58	90.02	89.66	87.25	86.51	85.87	85.27
K/S	0.23	0.66	0.75	0.86	1.00	1.16	1.39	1.67	1.86	2.18	2.36

3.3. Morphological characterization

Epoxy resin was used as a hosting agent to uphold varying concentrations of the phosphor nanoparticles. To accomplish a consistent spreading of NSA in the epoxy film, the supplied nanocomposites were exposed to sonication. The pigment-containing glazed polyepoxide nanocomposites were ultrasonically homogenized after adding the hardener to provide a uniform spreading of NSA. The prepared nanocomposites were applied to ceramics by a roller. Employing the top-down process, the pigment microparticles were converted into NSA, allowing for the formation of colorless coatings [45]. The sizes of NSA were determined by TEM, which shows dimensions of 9-18 nm, as demonstrated in **Figure 5**.

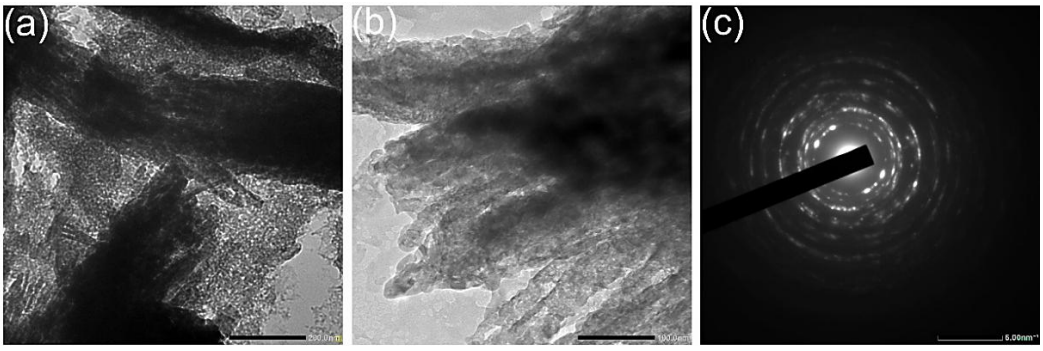


Figure 5. TEM examination (a-b) and SAED analysis (c) of NSA at various magnifications.

Figure 6(A) shows that the pigment micro powder, which was examined by SEM, has diameters ranging from 1 μm to 15 μm. **Figure 6(B)** displays the XRD pattern of NSA, which revealed a pure crystal phase of $SrAl_2O_4$ (JCPDS: 74-0794). The characteristic XRD signals were monitored at 19.62°, 28.05°, 28.94°, 29.57°, and 34.82°. A full integration of dopants in the $SrAl_2O_4$ crystal was confirmed by the absence of peaks for Dy and Eu [46]. According to Scherrer's equation [47], the estimated diameter of the NSA crystal was 14 nm. The chemical analysis of NSA was measured by EDX, which identified several elements as indicated in **Figures 6(C&D)**. These elements included dysprosium (2.51 wt%), europium (3.59 wt%), strontium (33.85 wt%), oxygen (36.47 wt%), and aluminum (23.57 wt%).

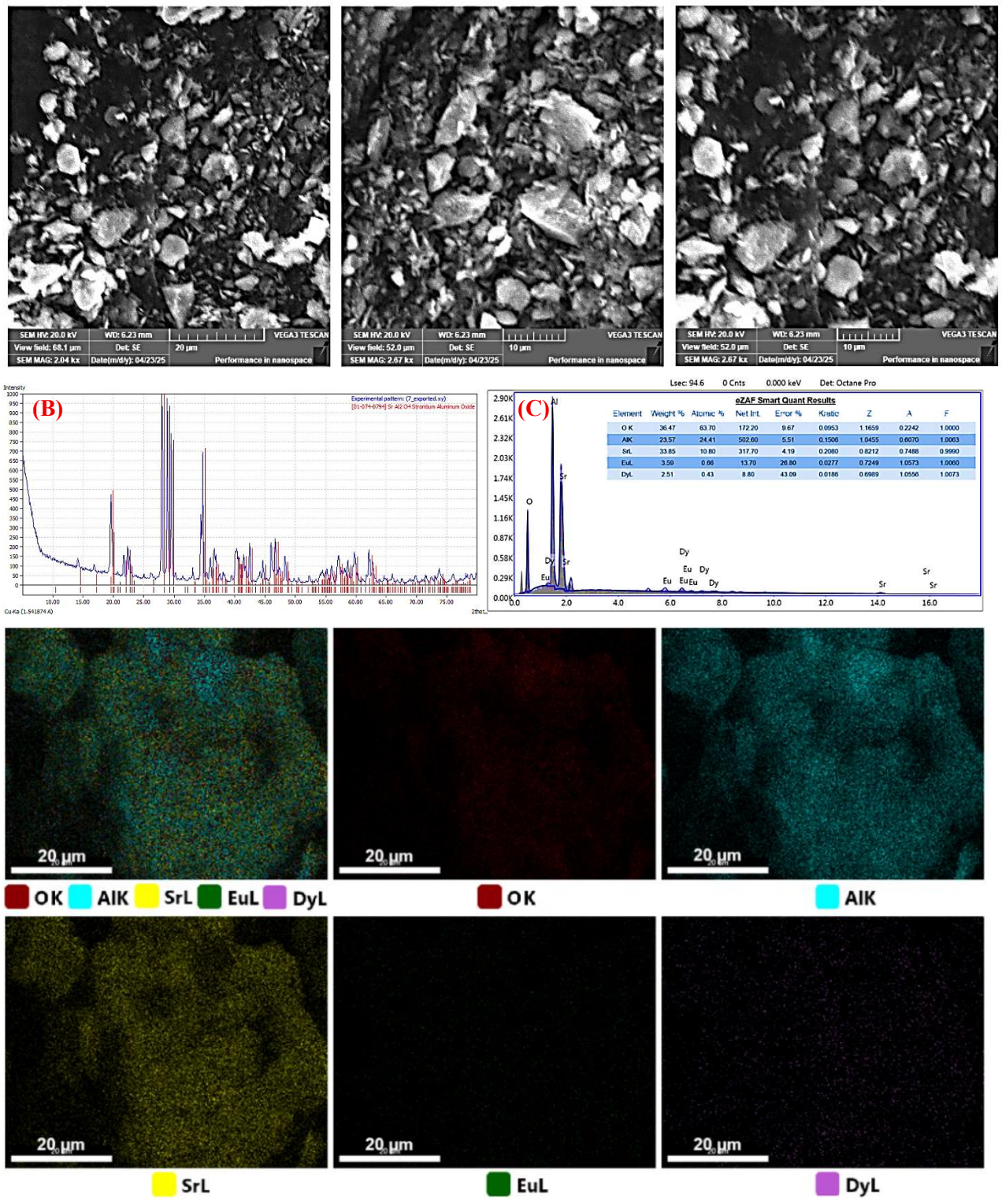


Figure 6. (A): SEM inspection of the phosphor microparticles. **(B):** XRD spectra of NSA (*top*) and its typical pattern (*bottom*). (C): EDX diagram of NSA. (D): Elemental analysis of NSA.

The mechanical performance of a composite can be enhanced by the reinforcement of polymers with glass fibers [48]. Glass fibers are distinguished by chemical stability, excellent electrical insulation, large surface area, thermal stability,

great tensile strength, and dimensional stability [49]. The glass fibers showed diameters of 50-220 nm, as illustrated in **Figure 7.**

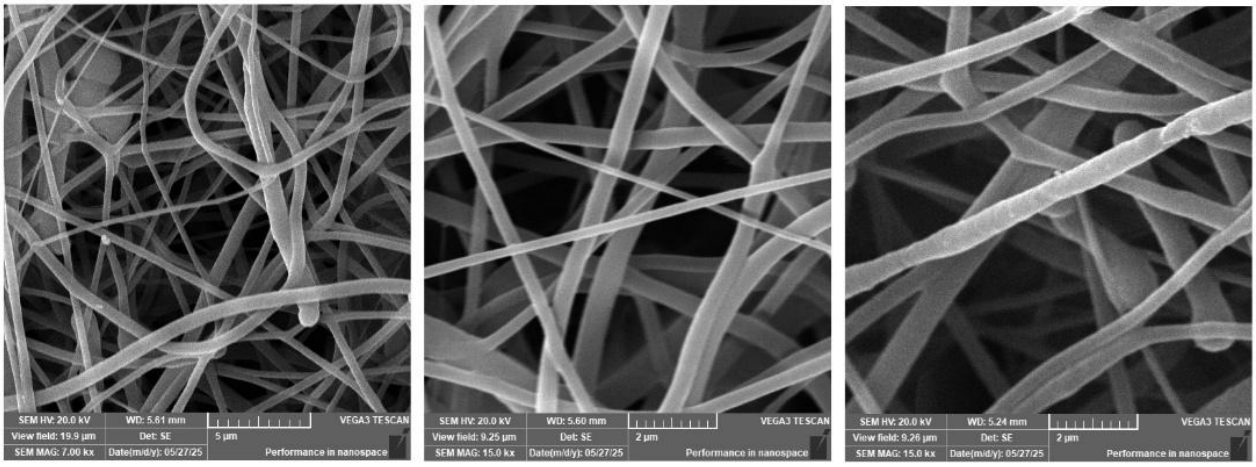


Figure 7. SEM examination of glass nanofibers.

SEM analysis reveals the morphology of luminescent ceramic, as illustrated in **Figure 8**. The surfaces of the NSA-integrated and NSA-free ceramics showed no significant differences. Additionally, increasing the NSA content did not affect the glazed NSA@EPR-coated ceramics. The elemental contents were analyzed by the EDX technique, confirming the existence of NSA in the glazed epoxy matrix. **Table 2** shows the chemical composition of the glazed polyepoxide coating evaluated at three distinct positions (P_1, P_2, and P_3), demonstrating identical elemental concentrations. This confirms that NSA is homogeneously distributed in the glazed epoxy layer. It was found that the elemental contents employed in the preparation process of the phosphor-embedded glazed polyepoxide were compatible with the elemental contents reported by EDX. In the luminescent film, the primary elements are silicon, oxygen, and carbon due to the usage of glazed polyepoxide as a host bulk. The minor elemental compositions include Dy, Al, Sr, Ti, and Eu, owing to the usage of NSA and TiO_2 as functional agents. Both XRF and EDX were utilized to measure the chemical contents of ceramics. A film of NSA_7 (13.26 cm^3) was analyzed using XRF, which revealed that it consisted of SrO (40.53 wt%) and Al_2O_3 (59.47 wt%). Due to their exceptionally low concentration, XRF could not identify Eu or Dy.

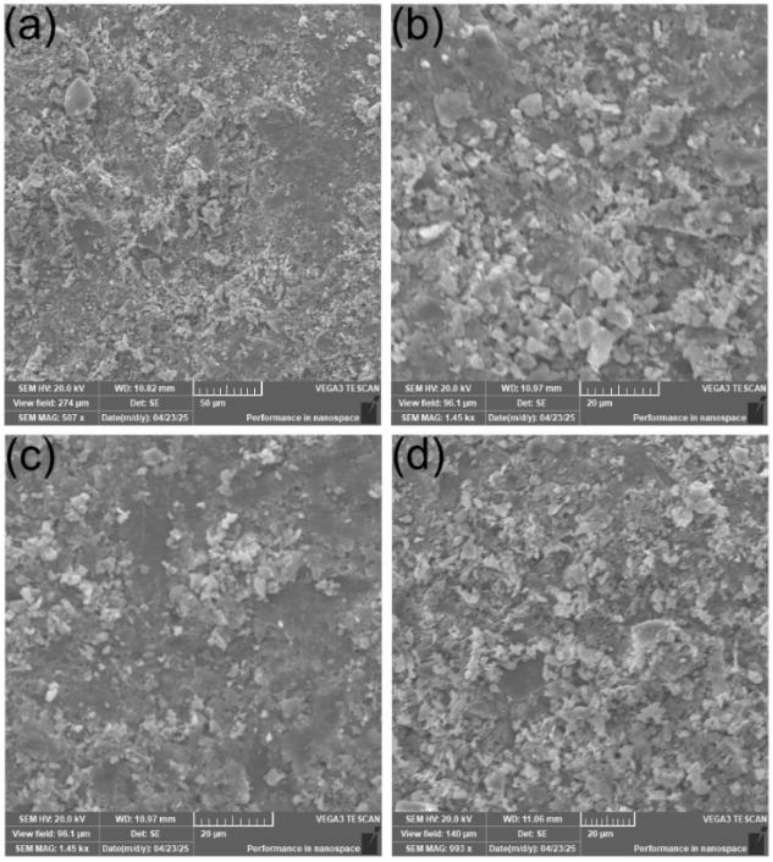


Figure 8. SEM investigation of treated ceramics: NSA_0 (a), NSA_1 (b), NSA_7 (c), and NSA_{10} (d).

Table 2. Elemental inspection (wt%) of ceramics at various positions (*p*).

Coating		C	O	Ti	Si	Sr	Al	Dy	Eu
NSA_0	P_1	78.06	14.47	2.25	4.70	–	2.52	–	–
	P_2	77.83	14.36	2.37	5.13	–	2.31	–	–
	P_3	77.31	14.90	2.68	4.41	–	2.70	–	–
NSA_1	P_1	77.10	15.09	2.39	4.22	0.19	2.85	0.07	0.09
	P_2	77.24	15.01	2.23	4.32	0.11	2.73	0.01	0.05
	P_3	77.39	15.56	2.20	4.06	0.15	2.27	0.04	0.13
NSA_7	P_1	66.10	16.03	1.88	3.41	5.15	8.06	0.09	0.28
	P_2	65.00	15.10	1.63	3.93	5.08	7.63	0.15	0.47
	P_3	66.51	16.31	1.91	3.06	5.01	7.80	0.07	0.33
NSA_{10}	P_1	62.58	17.36	1.36	3.39	6.23	9.53	0.20	0.35
	P_2	62.28	17.23	1.38	3.08	7.05	9.14	0.32	0.52
	P_3	62.56	17.05	1.73	3.12	6.10	9.82	0.15	0.47

3.4. Mechanical screening

The mechanical behavior of ceramics is significant to determine the durability of a coating. The glazed epoxy was primarily utilized to provide a practical surface with minimal roughness and maximum transparency. Consequently, the mechanical activity of coatings was examined by resistance to scratches and tensile tests. The films were scratched using sharpened pencils (6B-9H). The uncoated ceramic was unable to withstand scratches exceeding the 6B pencil. When evaluated with the B pencil, NSA showed resistance to scratches up to a B pencil. The ceramics showed

resistance to scratches up to F (NSA_0), H (NSA_1), H (NSA_2), H (NSA_3), H (NSA_4), 2H (NSA_5), 2H (NSA_6), 3H (NSA_7), 3H (NSA_8), 3H (NSA_9), and 3H (NSA_{10}). Thus, improved scratch resistance was monitored with a higher NSA ratio. **Figure 9** shows the tensile strength of optical films depending on the NSA content. The tensile strength of the polyepoxide films improved with raising the pigment ratio. This enhancement can be attributed to the large surface area of NSA, making it an effective stress transfer agent, generating plastic deformation [50]. Thus, increasing the quantity of NSA enhanced the tensile strength of the epoxy film. Additionally, the increased tensile of the NSA@EPR films with a greater pigment ratio could be ascribed to the creation of intermolecular electrostatic forces between NSA and polyepoxide, allowing for the creation of a 3D network [51].

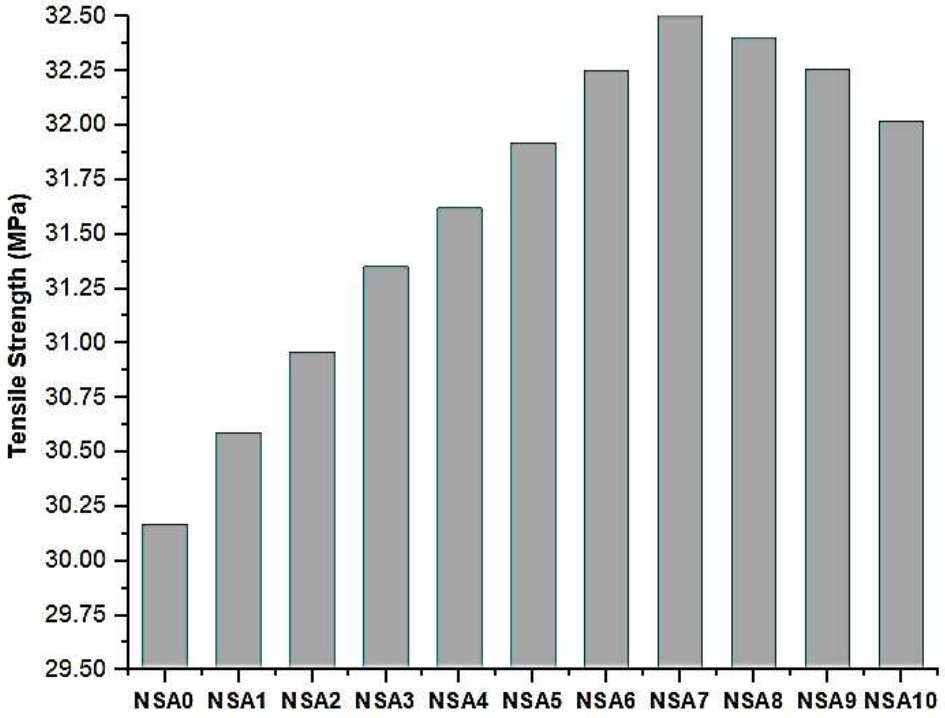


Figure 9. Tensile strength of cast films.

3.5. Hydrophobic measurements

Superhydrophobic coatings have shown a variety of applications, including anticorrosion, self-cleaning, and durable mechanical performance [52]. Owing to their ability to diminish the potential adhesion of pathogenic microorganisms, the superhydrophobic coatings can improve their antimicrobial activity [53]. As shown in **Figure 10**, no contact angle was observed for the uncoated sample. The addition of NSA increased the contact angle from 89.9° for NSA_0 to 109.5° for NSA_1. With a rise in the NSA concentration from NSA_1 to NSA_7, the contacting angle went up from 109.5° to 151.4°. This is attributed to the increased concentration of NSA, causing the surface to become more hydrophobic [54]. The contact angle values were found to slightly decrease with further raising the pigment content from NSA_7 to NSA_{10}. This could be ascribed to the surface roughness that remains stable or even decreases because the interstitial distance between the phosphor particles is reduced due to their extremely high content [55]. The hydrophobic

properties of coatings were assessed using sliding angles. With a rise in NSA concentration, the wetting properties were improved with increasing the NSA content, resulting in improved sliding angles.

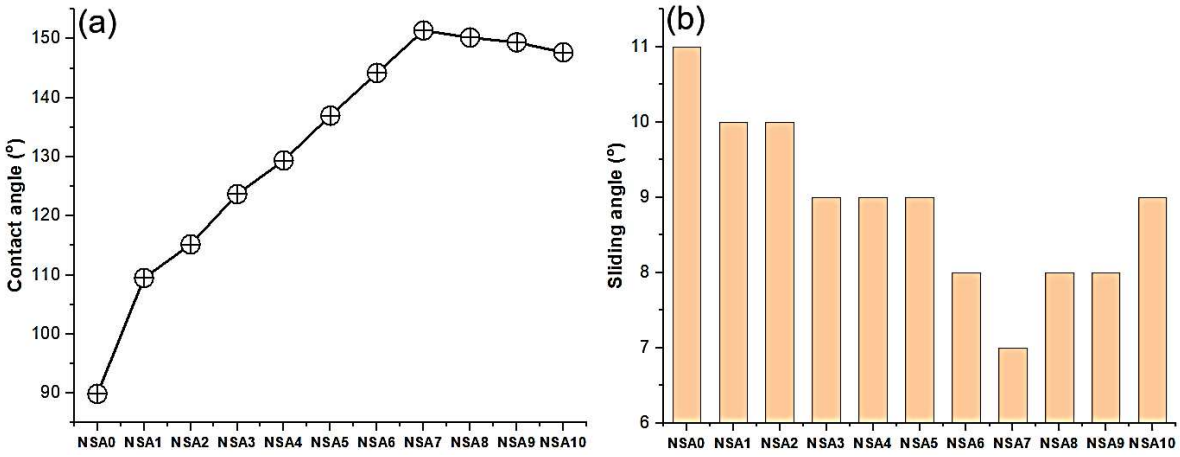


Figure 10. Hydrophobicity of coated ceramics, including contact angles (a) and sliding angles (b).

3.6. Ultraviolet shielding

There are many negative impacts of ultraviolet radiation on human health, such as accelerated aging, skin cancer, immune system suppression, and cataracts [56]. **Figure 11** displays the UV blocking of cast films. No ultraviolet shielding was detected for the NSA-free film (NSA_0). Because NSA has a high absorption capacity for UV radiation, NSA_1 outperformed the NSA-free film (NSA_0) in terms of ultraviolet absorption. As a result, glazier windows can be coated with the glazed polyepoxide to shield interiors from the harmful ultraviolet rays in the sunlight. A higher NSA concentration resulted in improved ultraviolet shielding. Glazier substrates were coated with the produced glazed NSA@EPR composites, resulting in energy-saving windows that glow in the dark. In the presence of strong sunlight rich with UV radiation, low UV rays penetrate the photoluminescent film and reach the building interior. The greenish emission of the glazed film produced by the UV radiation blocks up to 83% of sunlight from reaching inside the building. This is attributed to the NSA ability to function as a sunscreen due to its great efficacy to absorb ultraviolet light [57]. In the presence of weak sunlight, the glazed NSA@EPR material returns to its transparent state, letting a high ratio of sunlight reach the building interior.

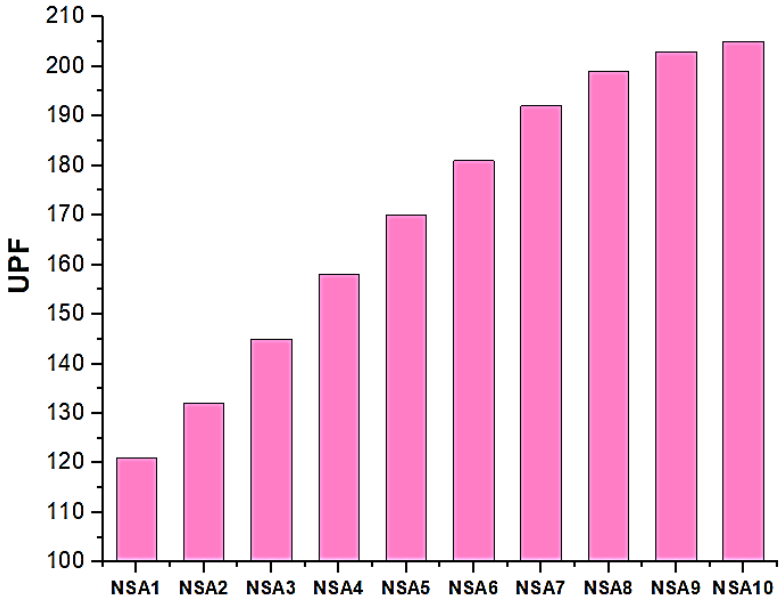


Figure 11. Ultraviolet shielding of cast films on glass slides.

3.7. Antimicrobial activity

Titanium dioxide-free and NSA-containing epoxy coatings **(Figure 12a)** showed weaker antimicrobial activity as compared to the TiO_2/NSA-containing glazed epoxy coatings **(Figure 12b)**. Titanium dioxide has shown high antimicrobial efficacy against numerous pathogens. It is characterized by high biocompatibility, chemical stability, and low toxicity to eukaryotic cells [58]. Additionally, NSA has shown antimicrobial efficacy against fungi and bacteria [59]. Thus, the coated ceramics showed inhibition of bacteria against *S. aureus* and *E. coli*. No bacterial inhibition was detected in either the uncoated sample or the NSA-free sample (NSA_0). Increasing NSA content enhanced antibacterial activity. The antimicrobial activity was observed to improve with raising the NSA ratio in the coated ceramics.

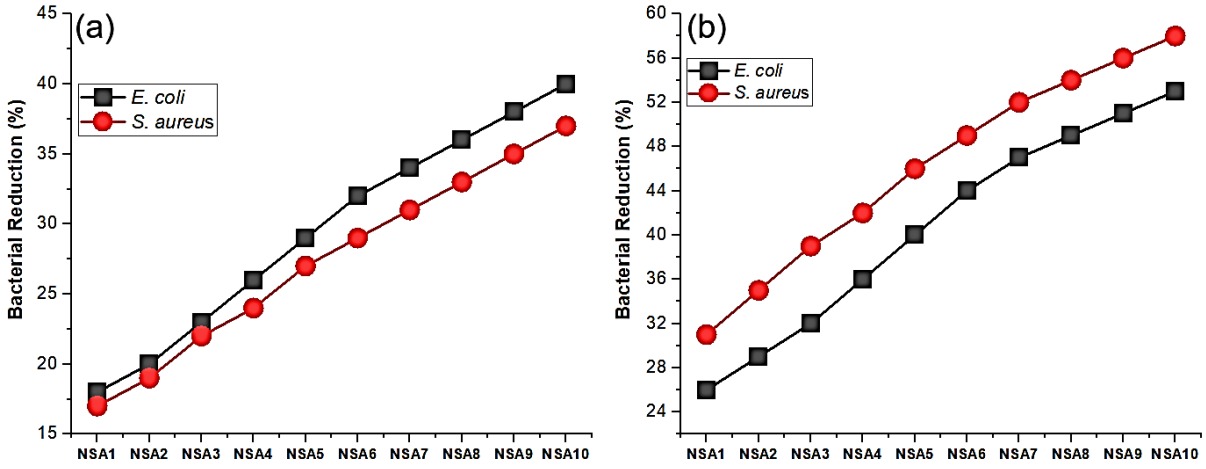


Figure 12. Antimicrobial activity of ceramics in the absence (a) and existence (b) of TiO_2.

4. Conclusions

The use of glazed epoxy integrated with phosphor nanoparticles allowed for efficient production of multifunctional luminescent ceramic. The glazed polyepoxide nanocomposites were reinforced with glass nanofibers (50-220 nm). To impart multifunctional properties, ceramics were coated with the produced nanocomposites containing varying concentrations of NSA. TEM analysis of the produced phosphor nanoparticles revealed diameters of 9-18 nm. The phosphor nanoparticles were consistently distributed in the epoxy matrix to achieve transparency in the coated layer. The results indicated that resistance to scratches and tensile strength of ceramics improved when the NSA concentrations rose. Improving the coating qualities and transparency relies on the NSA content being distributed efficiently in the glazed epoxy resin. Under ultraviolet light, the glazed epoxy sheets immobilized with NSA showed changes in color from transparent (365 nm) to greenish (519 nm). Fluorescence emissions were observed in multifunctional coatings at NSA contents of ≤1%, while prolonged phosphorescence was monitored when the total amounts of NSA were at or above 2%. Improving the hydrophobic properties of functional ceramics is essential. As the phosphor concentration increased, the contact and sliding angles were observed to increase from 89.9° to 151.4° and 11° to 7°, respectively, designating better hydrophobicity. Adding more NSA to the ceramic coating enhanced their ultraviolet shielding and antibacterial capabilities. The present method showed the capacity to produce functional coatings for ceramics and other surfaces, such as glasses and metals, for various applications, such as security encoding.

Acknowledgments

Authors are thankful for the National Research Centre, Cairo 12622, Egypt.

Author contributions

A.H.M., M.S.A., Y.A.A., and T.A.K. (Equal Contribution): Conceptualization, Methodology, Visualization, Investigation, Supervision, Data curation, Software, Validation, Writing-Original draft preparation, Writing-Reviewing and Editing.

Ethical Approval

Not applicable

Consent to Participate

All authors participated in this work.

Consent to Publish

All authors agree to publish.

Competing Interests

The authors declare that they have no competing interests.

Funding

Not applicable

Availability of data and materials

The data that support the findings of this study are available from the corresponding author upon reasonable request.

References

[1] N. Bar, and P. Chowdhury. A brief review on advances in rhodamine B based chromic materials and their prospects. *ACS Applied Electronic Materials* **4**(8), 3749-3771 (2022).

[2] L. Li, S.-H. Li, Z.-Y. Li, N.-N. Zhang, Y.-T. Yu, J.-G. Zeng, and Y. H.ua. Advances in viologen-based stimulus-responsive crystalline hybrid materials. *Coordination Chemistry Reviews* **518,** 216064 (2024).

[3] W. Si., S. Wang, Z.T. Yu, X. Dai, M. Guo, and Z. Guo. Super amphiphobic and photochromic coatings based on tungsten oxide can be utilized for repetitive writing under UV light in harsh environments. *Chemical Engineering Journal* **492**, 152232 (2024).

[4] G. Xiong, Z. Zhang, S. Hao, Q. Chen, C. Zhang, S. Zhang, K. Wang, and Y. Qi. Construction of novel fluorescent synergistic photocatalytic double Z-scheme photocatalyst for efficient antifouling of polydimethylsiloxane coatings. *Progress in Organic Coatings* **181,** 107575 (2023).

[5] Y. Wu, J. Gan, and X. Wu. Study on the silica-polymer hybrid coated SrAl2O4: Eu2+, Dy3+ phosphor as a photoluminescence pigment in a waterborne UV acrylic coating. *Journal of Materials Research and Technology* **13**, 1230-1242 (2021).

[6] M.S. Abdelrahman and T.A. Khattab. Recent advances in photoresponsive printing inks for security encoding applications. *Luminescence* **39**(6), e4800 (2024).

[7] J.-L. Zhao,, F.-H. Chen, Z. Ruan, Z.W. Cao, Y.-Q. Xu, Z.-Y. Cao, J.-X. Liu, M.-J. Lin, and M.-H. Li. Interlocking viologen-based lanthanide complexes for multifunctionality: Photochromism, electrochromism, photoluminescence, photomagnetism, and inkless printing and UV shielding applications. *Dyes and Pigments* **225**, 112100 (2024).

[8] G.M. Al-Senani and S.D. Al-Qahtani. Development of smart adhesive using lanthanide-doped phosphor and carboxymethyl cellulose-reinforced gum Arabic. *Spectrochimica Acta Part A: Molecular and Biomolecular Spectroscopy* **317**, 124397 (2024).

[9] Z. Yang,, J. Du, L.I.D.J. Martin, A. Feng, E. Cosaert, B. Zhao, W. Liu, R.V. Deun, H. Vrielinck, and D. Poelman. Designing photochromic materials with large luminescence modulation and strong photochromic efficiency for dual-mode rewritable optical storage. *Advanced Optical Materials* **9**(20), 2100669 (2021).

[10] Y. Chen, Z. Qiu, Y. Yao, Y. Liu, Z. Zhang, and Y. Li. Controlled Assembly of Single-Walled Carbon Nanotubes into Thin Films and Their Applications. *Advanced Functional Materials* 2426084 (2025).

[11] M. Li, M. Liu, F. Qi, F.R. Lin, and A.K.-Y. Jen. Self-assembled monolayers for interfacial engineering in solution-processed thin-film electronic devices: design, fabrication, and applications. *Chemical Reviews* **124**(5), 2138-2204 (2024).

[12] M.F. Ismail, M.A. Islam, B. Khorshidi, A. Tehrani-Bagha, and M. Sadrzadeh. Surface characterization of thin-film composite membranes using contact angle technique: Review of quantification strategies and applications. *Advances in Colloid and Interface Science* **299**, 102524 (2022).

[13] A.S. Altowyan,, J. Hakami, H. Algarni, and M. Shkir. Enhancing the optoelectronic properties of V2O5 thin films through Tb doping for photodetector applications. *Journal of Alloys and Compounds* **960**, 170911 (2023).

[14] M.M. Sabzehmeidani, S. Gafari, and M. Kazemzad. Concepts, fabrication and applications of MOF thin films in optoelectronics: A review. *Applied Materials Today* **38**, 102153 (2024).

[15] J. Farahbakhsh,, V. Vatanpour, M. Khoshnam, and M. Zargar. Recent advancements in the application of new monomers and membrane modification techniques for the fabrication of thin film composite membranes: A review. *Reactive and Functional Polymers* **166**, 105015 (2021).

[16] S. Misra and H. Wang. Review on the growth, properties and applications of self-assembled oxide–metal vertically aligned nanocomposite thin films—current and future perspectives. *Materials Horizons* **8**(3), 869-884 (2021).

[17] T. Bukreeva, V. Barachevsky, O. Venidiktova, P. Krikunova, and T. Pallaeva. Recent development of photochromic polymer capsules for smart materials. *Materials Today Communications* **38**, 107769 (2024).

[18] S. Sun,, Y. G.ao, N. Han, X.X. Zhang, and W. Li. Reversible photochromic energy storage polyurea microcapsules via in-situ polymerization. *Energy* **219**, 119630 (2021).

[19] M.T. Abdu,, T.A. Khattab, M.S. Abdelrahman, and M.S. Abdelrahman. Electrospinning of glass nanofibers to roughen a waterborne polyurethane coating toward smart applications. *Ceramics International* **50**(7), 11518-11527 (2024).

[20] M.H. El-Newehy,, B.M. Thamer, and M.M. Abdulhameed. Preparation of luminescent polyethylene plastic composite nano-reinforced with glass fibers. *Journal of Applied Polymer Science* **141**(14), e55189 (2024).

[21] M. Gouda, H.M. Abd El-Lateef, M.F. Abou Taleb, and M.M. Khalaf. Photoluminescent polypropylene nanofiber-supported polyethylene terephthalate integrated with strontium aluminate phosphor. *Journal of Photochemistry and Photobiology A: Chemistry* **453**, 115675 (2024).

[22] M.M. Aljohani, Preparation of polylactic acid reinforced with cellulose nanofibers toward photochromic self-healing adhesive for anti-counterfeiting applications. *International Journal of Biological Macromolecules* **259**, 129065 (2024).

[23] D.A.K. Alenazi, H.S. AlSalem, A.S. Alhawiti, M.S. Binkadem, A.A.H. Bukhari, N.A. Alhadhrami, R.A.S. Alatawi, and M.A. Abomuti. Development of strontium aluminate embedded photochromic cellulose hydrogel for mapping of fingermarks. *Inorganic Chemistry Communications* **152**, 110669 (2023).

[24] W. Li,, Y. Liu, and P. Ai. Synthesis and luminescence properties of red long-lasting phosphor Y_2O_2S: Eu^{3+}, Mg^{2+}, Ti^{4+} nanoparticles. *Materials Chemistry and Physics* **119**(1-2), 52-56 (2010).

[25] J. Kong and A. Meijerink. Identification and quantification of charge transfer in $CaAl_2O_4$: Eu^{2+}, Nd^{3+} persistent phosphor. *Advanced Optical Materials* **11**(15), 2203004 (2023).

[26] B. Walfort, N. Gartmann, J. Afshani, A. Rosspeintner, and H. Hagemann. Effect of excitation wavelength (blue vs near UV) and dopant concentrations on afterglow and fast decay of persistent phosphor $SrAl_2O_4$: Eu^{2+}, Dy^{3+}. *Journal of Rare Earths* 40(7), 1022-1028 (2022).

[27] M. El-Newehy, M.M. Abdulhameed, A.M. Karami, and H. El-Hamshary. Development of luminescent solution blown spun nanofibers from recycled polyester waste toward dual-mode fluorescent photochromism. *Journal of Polymers and the Environment* **30**(8), 3483-3494 (2022).

[28] A. Zanurin, N. A. Johari, J. Alias, H. Mas Ayu, N. Redzuan, and S. Izman. Research progress of sol-gel ceramic coating: A review. *Materials today: proceedings* **48**, 1849-1854 (2022).

[29] Z. Zhang,, Y. Huang, Q. Xie, G. Liu, C. Ma, and G. Zhang. Functional polymer–ceramic hybrid coatings: status, progress, and trend. *Progress in Polymer Science* 101840 (2024).
[30] Q. Zhu, M.H. Chua, P.J. Ong, J.J.C. Lee, K.L.O. Chin, S. Wang, D. Kai et al. Recent advances in nanotechnology-based functional coatings for the built environment. *Materials Today Advances* **15**, 100270 (2022).
[31] M.C. Chen, P.W. Koh, V.K. Ponnusamy, and S.L. Lee. Titanium dioxide and other nanomaterials based antimicrobial additives in functional paints and coatings. *Progress in Organic Coatings* **163**, 106660 (2022).
[32] D. Yan, J. Liu, Z. Zhang, Y. Wang, M. Zhang, D. Song, T. Zhang, J. Liu, F. He, and J. Wang. Dual-functional graphene oxide-based nanomaterial for enhancing the passive and active corrosion protection of epoxy coating. *Composites Part B: Engineering* **222**, 109075 (2021).
[33] A.-P. Bizymis and C. Tzia. Edible films and coatings: Properties for the selection of the components, evolution through composites and nanomaterials, and safety issues. *Critical Reviews in Food Science and Nutrition* **62**(31), 8777-8792 (2022).
[34] B. Ou, Y. Wang, and Y. Lu. A review on fundamentals and strategy of epoxy-resin-based anticorrosive coating materials. *Polymer-Plastics Technology and Materials* **60**(6), 601-625 (2021).
[35] M.M. Rahman and M.A. Islam. Application of epoxy resins in building materials: progress and prospects. *Polymer Bulletin* **79**(3), 1949-1975 (2022).
[36] S. Zhou, J. Yan, J. Chen, H. Yan, Y. Zhang, J. Huang, G. Zhao, Q. Zhang, and Y. Liu. Polydopamine/polyethyleneimine co-crosslinked graphene oxide for the enhanced tribological performance of epoxy resin coatings. *Journal of Materials Science & Technology* **136**, 13-20 (2023).
[37] A. Ruivo and C. Laia. CIE color coordinates for the design of luminescent glass materials." *Color Research & Application* **49**(1), 199-214 (2024).
[38] S.N.M.F. Han, M.M. Taha, M.R. Mansor, and M.A.A. Rahman. Investigation of tensile and flexural properties of kenaf fiber-reinforced acrylonitrile butadiene styrene composites fabricated by fused deposition modeling. *Journal of Engineering and Applied Science* **69**(1), 52 (2022).
[39] Z. Feng, W. Cai, J. Gao, G. Jiang, L. Qi, J. Li, Y. Hu, F. Chu, and W. Xing. Achieving scratch resistance and flame retardancy in transparent polycarbonate through P/N/Si synergistic coating. *Progress in Organic Coatings* **204**, 109247 (2025).
[40] S.C. Duru, C. Candan, and B. Nergis. Development of UV-Protective Hemp-Based Eco-Friendly Textiles. *Journal of Applied Polymer Science* e56737 (2025).
[41] P. Palmetshofer, S. Hengsbach, M. Guttmann, M. Worgull, and B. Weigand. Azimuthal variation of apparent contact angles on structured surfaces featuring micrometric ramps, pyramids and staggered cubes at two different inherent wettabilities. *Langmuir* **41**(11), 7312–7322 (2025).
[42] P. Phromphen, U. Sukatta, P. Rugthaworn, J. Boonyarit, P. Phoophat, N. Rungruangkitkrai, P. Tuntariyanond, N. Chartvivatpornchai, T. Apipatpapha, and R. Chollakup. Biosynthesis of silver nanoparticles enhanced antibacterial silk face covering. *Journal of Natural Fibers* **20**(2), 2212926 (2023).

[43] M.K. Sadannavar, X. Dong, A. Periyasamy, A. Jhatial, F. Rehman, F. A. Ghori, R.Z.A. Manj, and T. Zhao. Eco-friendly Sustainable Dyeing of Tencel Textiles with Plant-Based Bio-Mordant Using Dewberry Fruit Extract as a Source of Natural Dye. *Fibers and Polymers* **25**(10), 3829-3839 (2024).

[44] N.G. Al-Balakocy, M.S. Abdelrahman, H. Ahmed, A.A. Badawy, A.F. Ghanem, A.R. Wassel, Z. Wen, and T.A. Khattab. Photoluminescent and photochromic smart window from recycled polyester reinforced with cellulose nanocrystals. *Luminescence* **37**(9), 1575-1584 (2022).

[45] T. Tayebi, A. Baradaran-Rafii, A. Hajifathali, A. Rahimpour, H. Zali, A. Shaabani, and H. Niknejad. Biofabrication of chitosan/chitosan nanoparticles/polycaprolactone transparent membrane for corneal endothelial tissue engineering. *Scientific Reports* **11**(1), 7060 (2021).

[46] S.D. Al-Qahtani and G.M. Al-Senani. Glass nanofibers and lanthanide aluminate nanoparticles as reinforcement nanofillers for polyurethane composite toward smart applications. *Ceramics International* **50**(10), 16921-16928 (2024).

[47] S. Nasiri, M. Rabiei, A. Palevicius, G. Janusas, A. Vilkauskas, V. Nutalapati, and A. Monshi. Modified Scherrer equation to calculate crystal size by XRD with high accuracy, examples Fe_2O_3, TiO_2 and V_2O_5. *Nano Trends* **3**, 100015 (2023).

[48] A. Zucchelli, M.L. Focarete, C. Gualandi, and S. Ramakrishna. Electrospun nanofibers for enhancing structural performance of composite materials. *Polymers for Advanced Technologies* **22**(3), 339-349 (2011).

[49] M. Shams, N. Nezafati, D. Poormoghadam, S. Zavareh, A. Zamanian, and A. Salimi. Synthesis and characterization of electrospun bioactive glass nanofibers-reinforced calcium sulfate bone cement and its cell biological response. *Ceramics International* **46**(8), 10029-10039 (2020).

[50] G.M. Al-Senani and S.D. Al-Qahtani. Preparation of multifunctional and mechanically-reliable smart wood infiltrated with cellulose nanocrystal-reinforced polyvinyl alcohol nanocomposite. *International Journal of Biological Macromolecules* **273**, 133226 (2024).

[51] M. Gouda, H.M. Abd El-Lateef, M.F. Abou Taleb, and M.M. Khalaf. Polylactic acid film embedded with phosphor nanoparticles: Photochromic and afterglow biodegradable window and concrete. *Journal of Molecular Structure* **1300**, 137249 (2024).

[52] Z.Q. Tang, T. Tian, P.J. Molino, A. Skvortsov, D. Ruan, J. Ding, and Y. Li. Recent advances in superhydrophobic materials development for maritime applications. *Advanced Science* **11**(16), 2308152 (2024).

[53] A. Rajput, A. Mishra, A. Ali, R. Goswami, and N. Bhatt. Transparent superhydrophobic coating for copper metal and study of surface morphology and antimicrobial characteristics. *Colloids and Surfaces A: Physicochemical and Engineering Aspects* **684**, 133067 (2024).

[54] M.E. El-Naggar, A. Aldalbahi, T.A. Khattab, and M. Hossain. Facile production of smart superhydrophobic nanocomposite for wood coating towards long-lasting glow-in-the-dark photoluminescence. *Luminescence* **36**(8), 2004-2013 (2021).

[55] A.M. Aziz. Modification of wood lignin and integration with multifunctional polyester nanocomposite. *International Journal of Biological Macromolecules* **267,** 131466 (2024).

[56] Y. Ke and X.-J. Wang. TGFβ signaling in photoaging and UV-induced skin cancer. *Journal of Investigative Dermatology* **141**(4), 1104-1110 (2021).

[57] M. El-Newehy, B.M. Thamer, M.M. Abdul Hameed, and H. El-Hamshary. Photoluminescent polymer-based smart window reinforced with electrospun glass nanofibres. *Luminescence* **38**(8), 1511-1520 (2023).

[58] A. B. Younis, Y. Haddad, L. Kosaristanova, and K. Smerkova. Titanium dioxide nanoparticles: Recent progress in antimicrobial applications. *Wiley Interdisciplinary Reviews: Nanomedicine and Nanobiotechnology* **15**(3), e1860 (2023).

[59] E. Ahmed, D. Maamoun, M.S. Abdelrahman, T.M. Hassan, and T.A. Khattab. Imparting cotton textiles glow-in-the-dark property along with other functional properties: photochromism, flame-retardant, water-repellency, and antimicrobial activity. *Cellulose* **30**(6), 4041-4055 (2023).